The International Journal of Cardiovascular Imaging
https://doi.org/10.1007/s10554-024-03238-0

ORIGINAL PAPER

^{18}F-fluorodeoxyglucose PET-MR characterization of aortic inflammation in *ApoE*$^{-/-}$ mouse models of accelerated atherosclerosis: comparison of Western diet vs. uremia

Samuel Deshayes[1,2] · Pauline Ruello[2] · Christophe Simard[2] · Pierre-Antoine Dupont[2] · Caroline Bauge[2] · Ahmed Abbas[2] · Hubert de Boysson[1,2] · Achille Aouba[1] · Alain Manrique[2,3,4]

Received: 1 February 2024 / Accepted: 6 September 2024

Abstract

ApoE$^{-/-}$ mice are a widely used preclinical model of atherosclerosis, potentially accelerated by a Western diet (WD) or uremia. We aimed to compare hybrid ^{18}F-fluorodeoxyglucose (^{18}F-FDG) positron emission tomography-magnetic resonance (PET-MR) and immunostaining in *ApoE*$^{-/-}$ models of accelerated atherosclerosis. Five groups were studied: standard diet-fed *ApoE*$^{-/-}$ ($n=7$), standard diet-fed and uremic *ApoE*$^{-/-}$ ($n=7$), WD *ApoE*$^{-/-}$ ($n=7$), WD and uremic *ApoE*$^{-/-}$ ($n=6$), and control C57BL/6J mice ($n=6$). Uremia was induced by electrocoagulation of the right kidney at 8 weeks old, followed 2 weeks later by a contralateral nephrectomy. ^{18}F-FDG PET-MR imaging and histological staining (anti-CD4, -CD8, -CD11c, -CD20, -CD31, -CD68, -CD163, -interferon-γ, interleukin-1α, -1β, -6, -17 A antibodies) were performed in 18-week-old mice, i.e., 8 weeks after 5/6 nephrectomy and/or WD. ^{18}F-FDG uptake was similar in all groups. In contrast, histological staining highlighted higher percentages of CD8-, CD68-, or CD11c-positive cells in *ApoE*$^{-/-}$ aortic samples than in wild-type aortic samples. In addition, immunostaining revealed some differences between *ApoE*$^{-/-}$ mouse groups. Only the WD seemed to contribute to these differences. Using immunostaining, WD appeared to be a stronger accelerator of atherosclerosis than uremia. However, ^{18}F-FDG PET-MR imaging failed to demonstrate in vivo increased aortic glucose uptake in these models.

Keywords Atherosclerosis · *ApoE*$^{-/-}$ · PET-MR · Uremia · Western diet

Introduction

Atherosclerosis and its complications (stroke and myocardial infarction) are the worldwide leading cause of death [1]. It is now considered an inflammatory disorder induced by low-density lipoprotein (LDL) particles, implicating both innate and adaptive immunity [1]. This new paradigm led to the assessment of different immunosuppressive or immunomodulatory treatments in human atherosclerosis targeting neutrophils, lymphocytes, monocytes and/or their leading cytokines with colchicine [2, 3], methotrexate [4] or canakinumab [5]. Colchicine and canakinumab improved clinical outcomes in selected patients, decreasing the risk of cardiovascular events in secondary prevention by 15 to 30% [2, 3, 5]. However, as reported with interleukin-1 inhibitors and methotrexate, their use may be hampered by significant weight gain, potentially accelerating the course of atherosclerosis, or by cytolytic hepatitis [6, 7]. Hence, an optimal

Achille Aouba and Alain Manrique contributed equally to this work.

✉ Alain Manrique
manrique@cyceron.fr

[1] Department of Internal Medicine, Normandie Univ, UNICAEN, CHU de Caen Normandie, Caen 14000, France

[2] Normandie Univ, UNICAEN, UR4650 PSIR, CHU de Caen Normandie, Caen 14000, France

[3] Department of Nuclear Medicine, Normandie Univ, UNICAEN, CHU de Caen Normandie, Caen 14000, France

[4] UR4650 PSIR, GIP Cyceron, Campus Jules Horowitz, Boulevard Henri Becquerel, BP 5229, Caen 14074, France

Published online: 21 September 2024

and refined understanding of the pathophysiology of atherogenesis and the consequent development of new therapeutic targets remain necessary.

In *ApoE*$^{-/-}$ mice, the absence of apolipoprotein E (ApoE) leads to hypercholesterolemia and to the development of atherosclerotic lesions from 10 weeks of age [8, 9]. Positron emission tomography (PET) is a noninvasive method for the detection of aortic inflammation that has been used for assessing atherogenesis in vivo in *ApoE*$^{-/-}$ mice [10–14]. Hybrid PET-magnetic resonance (MR) imaging allows for quantitative or semiquantitative analysis of aortic glucose uptake within vascular structures by noncontrast MR angiography. Hence, in removing the life-threatening injected volumes of CT contrast, PET-MR is theoretically most fitted to the physiology of small animals.

Among the proposed methods to accelerate atherosclerosis in *ApoE*$^{-/-}$ mice, a high-fat high-cholesterol Western diet (WD) multiplies the burden of atherosclerotic lesions by approximately 3-fold [15] and increases the number of proinflammatory cells [16]. The reduction of the nephron mass of at least 50% also potentiates the development of atherosclerosis [17, 18], and subtotal 5/6 nephrectomy-induced uremia increases the area of atherosclerotic lesions 10-fold after 12 weeks of uremia [19]. Despite their high relevance for translational research, no study has compared the performances of these two methods in accelerating atherogenesis in *ApoE*$^{-/-}$ mice, especially by means of hybrid PET-MR imaging.

We therefore aimed to compare ^{18}F-fluorodeoxyglucose (^{18}F-FDG) PET-MR imaging and immunohistological findings in *ApoE*$^{-/-}$ mice, with or without WD or uremia, and in wild-type mice.

Materials and methods

Mice

Male C57BL/6 *ApoE*$^{-/-}$ (B6.129P2-*Apoe*^{tm1Unc}/J) and control C57BL/6J wild-type mice were purchased from The Jackson Laboratory (Sacramento, CA, USA) and Janvier Labs (Le Genest St. Isle, France), respectively, and housed in a temperature-controlled specific pathogenic free environment with *ad libitum* access to food and water. Five groups of mice were studied, including a control group of 6 standard diet-fed C57BL/6 mice. Twenty-seven *ApoE*$^{-/-}$ mice were randomly allocated to one of 4 groups: standard diet-fed *ApoE*$^{-/-}$ (SD, $n=7$), SD and uremic *ApoE*$^{-/-}$ (SD-U, $n=7$), WD *ApoE*$^{-/-}$ (WD, $n=7$), WD and uremic *ApoE*$^{-/-}$ (WD-U, $n=6$). Chronic renal failure was induced by electrocoagulation of the right kidney at 8 weeks old, followed by a contralateral nephrectomy two weeks later, as previously described [13]. Analgesia was obtained by preoperative subcutaneous injection of buprenorphine (0.05 mg/kg) and then every 12 h as long as needed. Mice were fed standard chow up to 10 weeks old, and then for the next 8 weeks, 14 mice continued on standard chow and 13 mice switched to WD (SAFE Western 1635 v35, SAFE Diet, Augy, France, made of 21.2% fat, 17% proteins, 48.5% carbohydrates, 0.2% total cholesterol) according to the experimental groups. The mice were separated according to the defined diet, but uremic mice were cohoused with nonuremic mice to decrease the cage effect. An additional analysis was performed to compare all mice that were fed an SD versus a WD and to compare all nonuremic mice to uremic mice.

All animal procedures were approved by the regional animal ethics committee (Comité d'Éthique NOrmand en Matière d'EXpérimentation Animale, CENOMEXA 054, n°29982) and were performed in accordance with the European directive 2010/63/EU on the protection of animals used for scientific purposes and specific French laws (decree n°2013–118). The study is reported in accordance with ARRIVE guidelines.

PET-MR imaging

Images were acquired in 18-week-old mice, i.e., 8 weeks after the introduction of uremia and/or WD, using a dedicated hybrid PET-MR 7T system (BioSpec 70/18, Bruker, Germany). The MR acquisition sequences consisted of a localizer, an axial 2D TOF FLASH angiography (TE: 1.657 ms, TR: 12 ms, 125 × 125 matrix, bandwidth: 700 Hz/pixel, flip angle: 80°, averages: 2, slice thickness: 0.6 mm, slices: 60), an axial T2 TurboRARE (TE: 24 ms, TR: 1720 ms, image size: 150 × 150, RARE factor: 5, averages: 8, slice thickness: 0.5 mm, slices: 30) and a whole-body FISP (TE: 2.6 ms, TR: 5.5 ms, flip angle: 10°, image size: 80 × 80, averages: 3, slice thickness: 0.5 mm, slices: 60). The 2D TOF imaging was gated to the ECG to avoid cardiac motion artifacts, and T2 TurboRARE was gated to the respiratory signal. MR images were used as landmarks to quantify ^{18}F-FDG uptake in vessels of interest.

The mice were fed a ketogenic diet for 2 days and then fasted 18 h before ^{18}F-FDG (Curium, Glisy, France) was intraperitoneally injected into conscious mice to decrease myocardial uptake [20–22]. Then, anesthesia was induced with 5% isoflurane gas and maintained with isoflurane 1–2% in an N_2O/O_2 mixture (2:1), and the mice were placed in a prone position headfirst in the PET-MR system. A static whole-body PET acquisition (15 min) was acquired 90 ± 1 min after the ^{18}F-FDG injection, with energy windows and coincidence windows of 357–664 keV and 5 ns, respectively. The axial scan length was 117 mm. The image

data were corrected for dead time, radioactive decay, attenuation, scatter and randoms, and sinograms were reconstructed using a 3-dimensional OSEM algorithm (number of iterations: 12, number of subsets: 16) into a 128×128 matrix (slice thickness 0.75 mm).

3D Slicer 4.11 (http://www.slicer.org/) with the PET-IndiC extension was used to analyze PET-MR images [23–26]. Alignment of the PET data to MR images was refined using a rigid transformation (6 degrees of freedom). The TOF sequences were used to manually draw volumes of interest (VOIs) encompassing the entire available portion of the ascending thoracic aorta, descending thoracic aorta, abdominal aorta and inferior vena cava. We divided the aorta into these three sections because atherosclerotic lesions in *ApoE*$^{-/-}$ mice do not develop at the same speed in each arterial segment, with the first lesions appearing in the thoracic aorta, particularly the aortic root, and because the division between ascending and descending thoracic aorta can lessen the impact of a possible spillover effect [9, 27]. Then, the VOIs of the aorta were dilated by the neighborhood method (8 neighbors) to include the vessel wall. The target-to-background ratio (TBR) was defined as the ratio of the maximum uptake within each VOI of the aorta and of the maximum uptake of vascular background measured in the inferior vena cava.

Blood analyses and ex vivo radioactivity measurement

Immediately after PET-MR imaging, blood samples were obtained by intracardiac puncture and collected in dry tubes while mice were under deep anesthesia. Analyses were performed by an external laboratory according to their internal protocols (LABÉO Frank Duncombe, Saint-Contest, France). Then, the mice were euthanized by decapitation under deep anesthesia. All precautions were taken to minimize suffering. After the aorta was removed, periaortic brown adipose tissue was removed and a piece at the thoracoabdominal junction was harvested, regardless of the PET-MR results, weighed and gamma counted with an ad hoc ^{18}F protocol for 60 s (Wizard 2470, PerkinElmer, Boston, MA, USA), 163 ± 8 min after the ^{18}F-FDG injection. The results were expressed as percentage of injected dose per gram of tissue (%ID/g).

Histological staining

Atherosclerotic lesions were revealed with Oil red O staining. Immunostaining was performed on a BenchMark XT (Ventana Medical Systems Inc., Tucson, AZ, USA). The following rabbit antibodies were used according to the manufacturers' protocols: anti-CD4 (1:50, Cell Signaling, catalog number: #25229), anti-CD8α (1:200, Cell Signaling, catalog number: #98941), anti-CD20 (1:50, Abcam, catalog number: #ab64088), anti-CD31 (1:100, Cell Signaling, catalog number: #77699), anti-CD11c (1:100, Cell Signaling, catalog number: #97585), anti-CD68 (1:600, Cell Signaling, catalog number: #97778), anti-CD163 (1:200, Abcam, catalog number: #ab182422), anti-interleukin (IL)-1β (1:150, Abcam, catalog number: #ab205924), anti-IL-1α (1:100, Abcam, catalog number: #ab7632), anti-IL-6 (1:100, ThermoFisher Scientific, catalog number: #BS-0782R), anti-IL-17 A (1:100, ThermoFisher Scientific, catalog number: #PA5-79470), and anti-interferon-γ (1:100, Abcam, catalog number: #ab216642). Bound antibodies were detected using avidin-biotin-peroxidase complex (ChromoMap DAB and OmniMap anti-Rabbit HRP, Roche Diagnostics, Meylan, France). Images were acquired using an Olympus VS120 slide scanner (Olympus, Tokyo, Japan) at 20× magnification. Tissue segmentation was manually performed by the same investigator (SD) using the QuPath software package (v0.2.3) [28], and data were expressed as the mean percentage of positive cells using the "Positive cell detection" option (optical density sum, Score compartment: DAB OD max with single threshold at 0.25) or as the mean percentage of positive area for the Oil red O staining (threshold set to 0.5 and smoothing sigma set to 1 with a full resolution of 0.35 µm/px).

Statistical analyses

Quantitative data were expressed as the mean ± standard error of the mean and analyzed using the nonparametric Mann–Whitney test, or, when more than two groups were compared, by the nonparametric Kruskal–Wallis test, followed if significant by Dunn's multiple comparison test. GraphPad Prism 7 (GraphPad Software Inc., San Diego, CA, USA) was used for statistical analyses. A p value < 0.05 was considered significant.

Results

Five groups of male mice were analyzed: SD *ApoE*$^{-/-}$ ($n = 7$), SD-U *ApoE*$^{-/-}$ ($n = 7$), WD *ApoE*$^{-/-}$ ($n = 7$), WD-U *ApoE*$^{-/-}$ ($n = 6$) and control C57BL/6 mice ($n = 6$). All experiments were performed in 18-week-old mice, with a mean weight of 29.85 ± 0.42 g.

Biological analyses

Blood total cholesterol levels were significantly higher in the WD *ApoE*$^{-/-}$ and WD-U *ApoE*$^{-/-}$ groups than in the control C57BL/6 mice ($p < 0.05$, Table 1). Blood triglyceride levels

Table 1 Results of biological analyses

	SD ($n=7$)	SD-U ($n=7$)	WD ($n=7$)	WD-U ($n=6$)	WT ($n=6$)	p value	Dunn's test
Total cholesterol (g/L)	10.12 ± 1.23 ($n=5$)	8.57 ± 0.68 ($n=3$)	13.52 ± 1.64 ($n=5$)	18.01 ± 2.33 ($n=5$)	1.15 ± 0.09	**0.002**	WD vs. WT* WD-U vs. WT**
Triglycerides (g/L)	1.47 ± 0.10 ($n=4$)	1.68 ± 0.11 ($n=2$)	1.25 ± 0.28 ($n=3$)	1.21 ± 0.19 ($n=4$)	0.61 ± 0.07	**0.02**	SD-U vs. WT*
Calcium (mg/L)	92.85 ± 1.60 ($n=4$)	96.30 ± 0.70 ($n=2$)	92.97 ± 1.11 ($n=3$)	97.60 ± 3.79 ($n=4$)	90.78 ± 0.98	0.17	
Phosphorus (mg/L)	109.45 ± 6.80 ($n=4$)	129.70 ± 8.60 ($n=2$)	139.73 ± 1.33 ($n=3$)	144.20 ± 6.01 ($n=4$)	114.57 ± 5.54	**0.02**	NS

Values are displayed as the mean (± SEM), and significant values (i.e., p value < 0.05) are displayed in bold. SD: Standard diet ApoE$^{-/-}$; *SD-U: Standard diet + uremic ApoE$^{-/-}$*; WD: Western diet ApoE$^{-/-}$; *WD-U: Western diet + uremic ApoE$^{-/-}$*; Wild-type; *NS: Not significant with Dunn's multiple comparison test value. *: $p < 0.05$, **: $p < 0.01$*

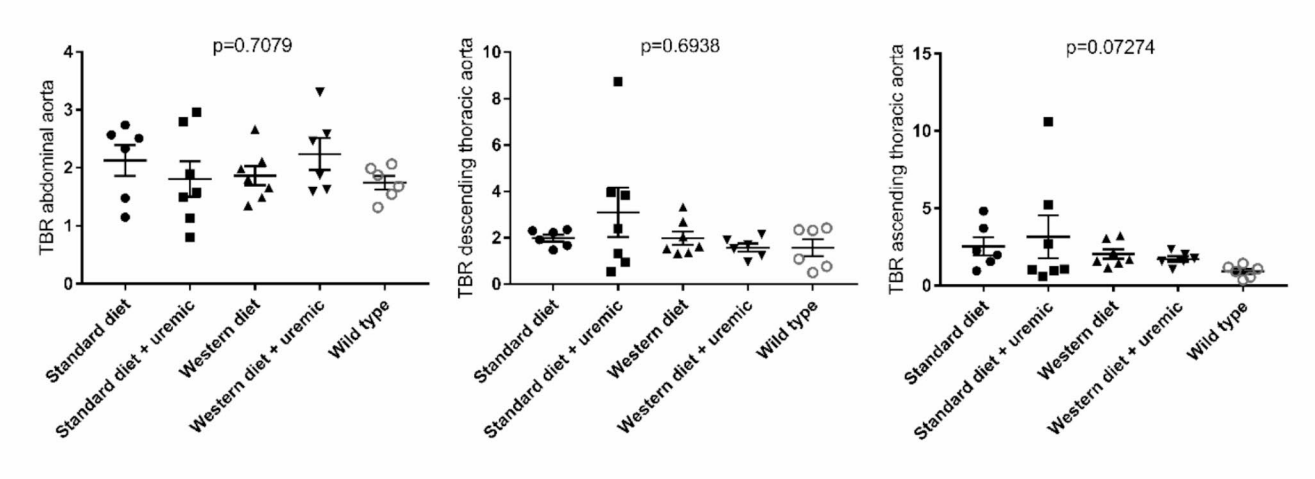

Fig. 1 Results of ^{18}F-FDG PET quantification in 18-week-old standard diet-fed *ApoE*$^{-/-}$ ($n=6$), standard diet-fed and uremic *ApoE*$^{-/-}$ ($n=7$), Western diet-fed *ApoE*$^{-/-}$ ($n=7$), Western diet-fed and uremic *ApoE*$^{-/-}$ ($n=6$) or wild-type C57BL/6J mice ($n=6$)

were significantly higher in SD-U *ApoE*$^{-/-}$ mice than in control C57BL/6 mice ($p=0.042$).

PET-MR imaging and ex vivo radioactivity measurement

The mice received a mean of 22.15 ± 0.74 MBq of ^{18}F-FDG, without a significant difference among the five groups ($p=0.54$). An accidental intracolic injection of ^{18}F-FDG prevented the analysis of the images for one mouse in the SD *ApoE*$^{-/-}$ group. No significant difference was found between groups regarding the TBR, regardless of the aortic segment (Figs. 1 and 2). The results were similar with the mean uptake within each VOI (see Online Resource 1). The heart uptake was similar between groups ($p=0.13$, see Online Resource 2).

In addition, no significant differences were found regarding the radioactivity measured by gamma counting: 1.7 ± 0.49%ID/g in the SD *ApoE*$^{-/-}$ group ($n=2$), 5.2 ± 0.83%ID/g in the SD-U *ApoE*$^{-/-}$ group ($n=5$), 4.7 ± 0.81%ID/g in the WD *ApoE*$^{-/-}$ group ($n=7$), 4.3 ± 0.62%ID/g in the WD-U *ApoE*$^{-/-}$ group ($n=5$) and 2.8 ± 0.62%ID/g in the control C57BL/6 mice ($n=6$), $p=0.07$.

Histological staining

Because the results for thoracic or abdominal segments did not add specific relevance, the results for these segments were combined (Table 2). There were significantly more positive cells marked by anti-CD8 and anti-CD11c in WD-U *ApoE*$^{-/-}$ mice than in control C57BL/6 mice ($p=0.042$ and 0.018, respectively) (see Online Resource 3). In contrast, there was a decreased proportion of positive cells marked by CD31 in the SD *ApoE*$^{-/-}$ group and in the SD-U *ApoE*$^{-/-}$ group compared with the control C57BL/6 mice ($p=0.007$ and $p=0.002$, respectively). There was also a decreased percentage of IL-17 A-positive cells in the SD *ApoE*$^{-/-}$ group and in the SD-U *ApoE*$^{-/-}$ group compared with the control C57BL/6 mice ($p=0.0004$ and $p=0.003$,

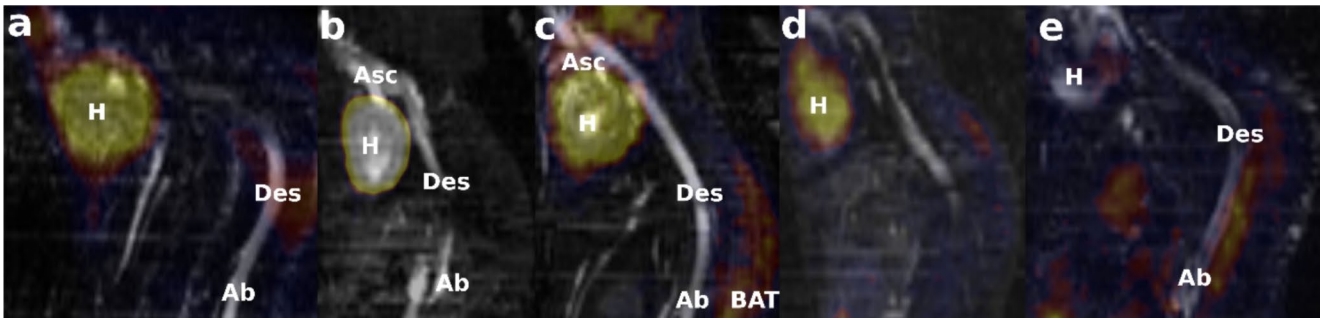

Fig. 2 Representative ^{18}F-FDG PET-MR imaging (sagittal sections of 2D TOF FLASH MR angiography sequences). **a**: standard diet *ApoE*$^{-/-}$ mice; **b**: standard diet and uremic *ApoE*$^{-/-}$ mice; **c**: Western diet *ApoE*$^{-/-}$ mice; **d**: Western diet and uremic *ApoE*$^{-/-}$ mice; **e**: wild-type C57BL/6J mice; **H**: heart; Ab: abdominal aorta; Des: descending thoracic aorta; Asc: ascending thoracic aorta; BAT: paravertebral brown adipose tissue

Table 2 Results of histological staining of mouse whole aortas in each group

	SD ($n=7$)	SD-U ($n=7$)	WD ($n=7$)	WD-U ($n=6$)	WT ($n=6$)	p value	Dunn's test
CD4	0.85 ± 0.26 ($n=6$)	1.01 ± 0.46	1.63 ± 0.56	4.62 ± 2.11	0.42 ± 0.17	0.38	-
CD8	1.88 ± 0.42	1.80 ± 0.68	7.08 ± 3.00	8.48 ± 3.86	1.04 ± 0.52	**0.038**	WD-U vs. WT*
CD11c	2.21 ± 0.96	2.66 ± 1.25	7.59 ± 2.61	10.09 ± 1.33	0.78 ± 0.28	**0.005**	WD-U vs. WT*
CD20	0.48 ± 0.29 ($n=6$)	0.48 ± 0.19	2.80 ± 1.64	4.91 ± 3.02	0.62 ± 0.45	0.17	-
CD31	30.91 ± 5.70	25.34 ± 6.16	45.53 ± 3.78	43.11 ± 2.87	59.41 ± 2.98	**0.002**	SD vs. WT** SD-U vs. WT**
CD68	1.26 ± 0.53	2.00 ± 0.62	4.18 ± 1.21	13.43 ± 4.51	0.46 ± 0.34	**0.002**	WD-U vs. SD* WD-U vs. WT**
CD163	4.77 ± 3.88	1.17 ± 0.38	5.10 ± 1.69	8.10 ± 2.79	2.09 ± 0.45	0.14	-
Interferon-γ	1.11 ± 0.30	1.66 ± 0.45	14.03 ± 3.50	11.13 ± 2.58	3.44 ± 1.09	**0.0002**	SD vs. WD** SD vs. WD-U** SD-U vs. WD* SD-U vs. WD-U*
Interleukin-1α	3.15 ± 1.01	3.65 ± 1.44	8.09 ± 4.35	17.74 ± 5.10	3.84 ± 0.71	**0.037**	SD-U vs. WD-U*
Interleukin-1β	10.83 ± 5.25	4.21 ± 2.26	10.84 ± 4.21	13.82 ± 4.55	2.16 ± 0.78	**0.035**	NS
Interleukin-6	3.38 ± 1.48	1.67 ± 0.43	10.73 ± 3.83	12.63 ± 4.06	6.10 ± 1.47	**0.002**	SD-U vs. WD* SD-U vs. WD-U**
Interleukin-17 A	10.05 ± 1.52	11.00 ± 2.04	28.56 ± 3.00	26.35 ± 4.42	43.35 ± 4.93	**< 0.0001**	SD vs. WT*** SD vs. WD* SD-U vs. WT**
Oil red O staining[1]	4.18 ± 1.54 ($n=5$)	5.50 ± 1.13 ($n=6$)	7.35 ± 0.91 ($n=6$)	10.01 ± 2.13 ($n=2$)	3.13 ± 0.70	**0.029**	NS

Unless indicated, values are displayed as the mean percentage of positive cells (± SEM). [1] Expressed as the mean percentage of positive area (± SEM). Significant values (i.e., p value < 0.05) are displayed in bold. SD: Standard diet *ApoE*$^{-/-}$; SD-U: Standard diet + uremic *ApoE*$^{-/-}$; WD: Western diet *ApoE*$^{-/-}$; WD-U: Western diet + uremic *ApoE*$^{-/-}$; Wild-type; NS: Not significant with Dunn's multiple comparison test value. *: $p < 0.05$, **: $p < 0.01$ ***: $p < 0.001$

respectively) and in the SD *ApoE*$^{-/-}$ group compared with the WD *ApoE*$^{-/-}$ group ($p=0.032$). Regarding anti-CD68 staining, there were significantly more positive cells in the WD-U *ApoE*$^{-/-}$ group than in the SD *ApoE*$^{-/-}$ group ($p=0.026$) or the control C57BL/6 group ($p=0.002$). For IL-6 staining, the WD *ApoE*$^{-/-}$ group and the WD-U *ApoE*$^{-/-}$ group had significantly more positive cells than the SD-U *ApoE*$^{-/-}$ group ($p=0.022$ and 0.006, respectively). There was also an increased proportion of interferon-γ-positive cells in the WD *ApoE*$^{-/-}$ group and in the WD-U *ApoE*$^{-/-}$ group compared with the SD *ApoE*$^{-/-}$ group ($p=0.002$ and 0.005, respectively) and in the SD-U *ApoE*$^{-/-}$ group ($p=0.013$ and 0.029, respectively). The results with the anti-IL-1α antibody showed an increased proportion of positive cells in the WD-U *ApoE*$^{-/-}$ group compared with the SD-U *ApoE*$^{-/-}$ group ($p=0.047$). The results regarding the anti-IL-1β and the Oil red O staining were different between groups ($p=0.035$ and 0.029, respectively), but the p values with the *post hoc* Dunn's multiple comparison test were not significant.

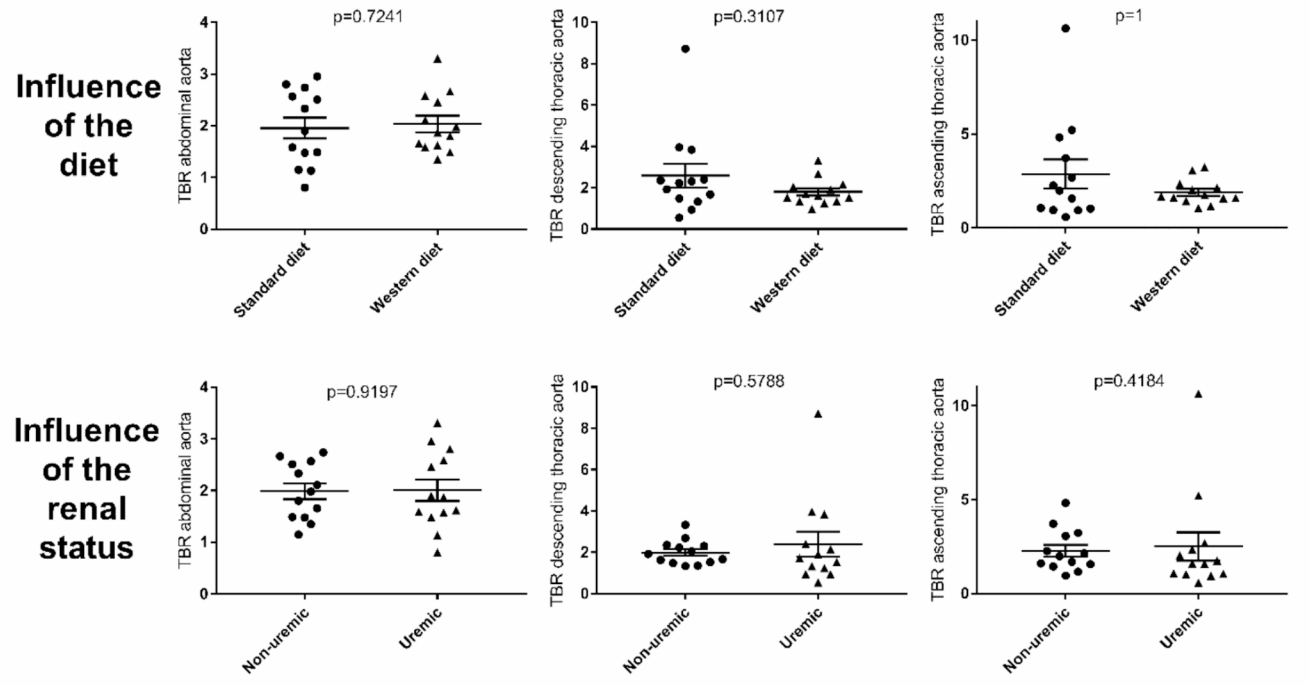

Fig. 3 Results of ^{18}F-FDG PET quantification in 18-week-old ApoE$^{-/-}$ mice according to their diet or renal status. Upper line: standard diet ($n=13$) versus Western diet ($n=13$)-fed ApoE$^{-/-}$ mice. Bottom line: nonuremic ($n=13$) versus uremic ($n=13$) ApoE$^{-/-}$ mice

Table 3 Histological staining results of mouse whole aortas according to diet or renal status

	Standard diet-fed *ApoE*$^{-/-}$ ($n=14$)	Western diet-fed *ApoE*$^{-/-}$ ($n=13$)	*p* value	Nonuremic *ApoE*$^{-/-}$ ($n=14$)	Uremic *ApoE*$^{-/-}$ ($n=13$)	*p* value
CD4	0.94 ± 0.27 ($n=13$)	3.01 ± 1.06	0.24	1.27 ± 0.33 ($n=13$)	2.68 ± 1.09	0.97
CD8	1.84 ± 0.39	7.73 ± 2.31	**0.015**	4.48 ± 1.62	4.89 ± 1.98	0.74
CD11c	2.43 ± 0.76	8.74 ± 1.52	**< 0.001**	4.90 ± 1.53	6.09 ± 1.38	0.80
CD20	0.48 ± 0.16 ($n=13$)	3.78 ± 1.60	**0.038**	1.73 ± 0.92 ($n=13$)	2.53 ± 1.47	0.40
CD31	28.12 ± 4.11	44.41 ± 2.36	**0.008**	38.22 ± 3.86	33.54 ± 4.29	0.49
CD68	1.63 ± 0.41	8.45 ± 2.47	**0.002**	2.72 ± 0.75	7.28 ± 2.59	0.16
CD163	2.97 ± 1.94	6.49 ± 1.56	**0.015**	4.94 ± 2.03	4.37 ± 1.59	0.99
Interferon-γ	1.38 ± 0.27	12.69 ± 2.18	**< 0.0001**	7.57 ± 2.46	6.03 ± 1.79	0.95
Interleukin-1α	3.40 ± 0.85	12.54 ± 3.47	**0.013**	5.62 ± 2.25	10.15 ± 3.11	0.33
Interleukin-1β	7.52 ± 2.90	12.21 ± 2.99	**0.038**	10.83 ± 3.23	8.64 ± 2.70	0.84
Interleukin-6	2.52 ± 0.78	11.61 ± 2.68	**< 0.0001**	7.06 ± 2.22	6.73 ± 2.39	0.80
Interleukin-17 A	10.52 ± 1.23	27.54 ± 2.50	**< 0.0001**	19.30 ± 3.03	18.09 ± 3.12	0.99
Oil red O staining[1]	4.90 ± 0.91 ($n=11$)	8.01 ± 0.89 ($n=8$)	**0.033**	5.91 ± 0.95 ($n=11$)	6.63 ± 1.18 ($n=8$)	0.60

Unless indicated, values are displayed as the mean percentage of positive cells (±SEM). 1 Expressed as the mean percentage of positive area (±SEM). Significant values (i.e., p value <0.05) are displayed in bold

To compare the respective contribution of each intervention, an analysis compared all *ApoE*$^{-/-}$ mice that were fed with an SD versus a WD, regardless of their renal status, and compared all nonuremic mice to uremic mice, regardless of their diet. The TBR, regardless of the aortic segment, was comparable between SD and WD mice and between nonuremic mice and uremic mice (Fig. 3). Similarly, no significant results were found by gamma counting ($p=0.17$ and 0.11, respectively). Regarding histological staining (Table 3), no significant differences were observed between nonuremic and uremic mice. In contrast, when combining the results for the thoracic and abdominal aortas, each staining was significantly higher in WD mice than in SD mice, except for the CD4 antibody.

Discussion

To our knowledge, this is the first study assessing two frequently used methods of accelerated atherosclerosis in *ApoE*$^{-/-}$ mice. We found that with its current sensitivity, our ^{18}F-FDG PET protocol at the 8-week follow-up did not detect metabolic remodeling within the aortic wall, whereas inflammation was revealed by immunostaining. In addition, this vessel wall inflammation was found only in WD mice.

The similarity of aortic ^{18}F-FDG uptake assessed by ^{18}F-FDG uptake or gamma counting between all groups, including the wild-type mice, was previously reported. Indeed, in the study by Ahmed et al. [11]., the aortic ^{18}F-FDG uptake was similar in WD *ApoE*$^{-/-}$ mice or in WD wild-type mice of 16 and of 20 weeks of age. In addition, in the study by Hag et al. [10]., aortic ^{18}F-FDG uptake, assessed by SUV_{mean} and gamma counting, was significantly higher in high-fat diet-fed *ApoE*$^{-/-}$ mice than in SD *ApoE*$^{-/-}$ mice after 16 weeks of diet but not after only 8 weeks. Similarly, in the study by Zhao et al. [12]., gamma counting of aortic ^{18}F-FDG uptake was similar in high fat, high cholesterol diet-fed *ApoE*$^{-/-}$ mice and in high fat, high cholesterol diet-fed wild-type mice compared with SD wild-type mice after 5 weeks of diet but was higher after 13 weeks of diet. The study by Laurberg et al. [14]. even suggests that aortic ^{18}F-FDG uptake is lower in nonatherosclerotic segments of the aorta than in advanced atherosclerotic lesions. Taken together, these results emphasized the lack of sensitivity of ^{18}F-FDG PET in assessing aortic inflammation in *ApoE*$^{-/-}$ mice, even when using a hybrid PET-MR approach. We have chosen a study endpoint of 8 weeks after the accelerated atherosclerosis method because intralesional macrophages at the early stage of foam cell formation are responsible at least in part for ^{18}F-FDG uptake [29] and because atherosclerotic lesions can be histologically detected as early as 3 weeks of WD [9] and as 6 weeks of uremia [30]. But, based on the results, it might be possible that our study endpoint was too early for demonstrating differences between groups. Although PET acquisition 3 h after ^{18}F-FDG injection has been reported to optimize the quantitation of atherosclerotic plaque inflammation in humans by decreasing blood pool activity [31], our PET acquisition 90 min after ^{18}F-FDG injection is in line with previous studies, with a delay ranging from 60 to 120 min after injection [12, 32]. In addition, to our knowledge, no study comparing different ^{18}F-FDG PET acquisition times has been performed in the *ApoE*$^{-/-}$ mouse model.

In contrast to metabolic imaging, histological staining clearly highlighted differences between *ApoE*$^{-/-}$ versus wild-type mice. As expected, because of the involvement of CD8^{+} cells and macrophages in the pathophysiology of atherosclerosis [33], more CD8- and CD68-positive cells were found in *ApoE*$^{-/-}$ mice than in wild-type mice, but the difference was significant only in the WD-U group. This group also exhibited more CD11c-positive cells, a phenotypic marker that is expressed by dendritic cells that exert both pro- and antiatherosclerotic functions but also by other cells, especially the monocyte-macrophage lineages [34]. Of note, the staining of CD163, a marker of anti-inflammatory and atheroprotective macrophages [35], is similar between groups, contrary to the results with the anti-CD68 antibody that is expressed on both pro- and anti-inflammatory macrophages.

In addition, immunostaining also revealed some differences between *ApoE*$^{-/-}$ mouse groups. Indeed, higher proportions of CD68-, interferon-γ-, IL-1α- and IL-6-positive cells were found in WD *ApoE*$^{-/-}$ mice and/or in WD-U *ApoE*$^{-/-}$ mice than in SD *ApoE*$^{-/-}$ and/or in SD-U *ApoE*$^{-/-}$ mice. Although some atheroprotective functions have been described for interferon-γ and IL-6, these cytokines and IL-1α are mainly considered atherogenic [36–38].

Two other features seem paradoxical. CD31, an adhesion molecule that is expressed in particular by endothelial cells, participates in the development of atherosclerotic lesions by sensing shear stress and through the transmigration of leukocytes. Therefore, double knockout *ApoE*$^{-/-}$/*CD31*$^{-/-}$ mice exhibit a significant reduction in atherosclerotic lesions [39]. We found that SD *ApoE*$^{-/-}$ and SD-U *ApoE*$^{-/-}$ mice have fewer positive CD31 cells within the aortic wall than control C57BL/6 mice. This may be secondary to the decreased expression of CD31 within the endothelial layer from 6 weeks to 16–20 weeks in this model, in parallel with the evolution of atherosclerotic lesions from the fatty to fibrous stage [40]. In addition, some proinflammatory cytokines can be responsible for both CD31 internalization and decreased synthesis, as shown with tumor necrosis factor-α and interferon-γ [41, 42]. The role of IL-17 A in atherogenesis is controversial, with both atherogenic and atheroprotective functions depending on the studies [43]. Indeed, IL-17 A may be involved in the early stage of atherosclerosis development and may explain a different percentage of positive cells among *ApoE*$^{-/-}$ mouse groups. Of note, the staining by anti-IL-17 A antibody was mainly localized in endothelial cells, which is unusual and may suggest a lack of specificity of the antibody.

In this study, the WD groups of mice exhibited a higher percentage of inflammatory cells than the SD groups. In contrast, the induced uremia did not seem to increase inflammatory cells. In line with these findings, no infiltration by B or T cells has been observed in previous studies with uremic mice [17, 44]. Previous results are controversial regarding the involvement of macrophages, demonstrating [45, 46] or not [18, 30] an increased macrophage content in atherosclerotic lesions. Uremia, although contradicted by some studies [17, 44], contributes to accelerating the calcification

processes as previously described [30, 47], including by our team [13]. Therefore, it may be possible that uremia leads to arterial mineralization, but perhaps with a lesser inflammatory component. Of note, the mice were separated according to the defined diet, but uremic mice were cohoused with nonuremic mice. The gut microbiota is involved in atherosclerosis [48], and this cohousing may have led a partial normalization of fecal microbiota in these two latter groups [49], which may explain some of our results.

Our study has several limitations. Besides the small number of mice within each group resulting in a lack of statistical power, the PET acquisition time point at 90 min and the endpoint 8 weeks after the introduction of the method to accelerate atherosclerosis, previously discussed, we only studied male mice, whereas atherosclerotic lesions are larger and more advanced in females in 14- to 16-week-old uremic and nonuremic *ApoE*$^{-/-}$ mice [30, 50]. We did not assess other radionuclides that could be of interest in atherosclerosis, such as ^{18}F-sodium fluoride, which targets active vascular microcalcifications and is not affected by myocardial uptake [13, 51, 52]. We have chosen *ApoE*$^{-/-}$ mice over other models, notably rats, because of the extensive study of this model in atherosclerosis, even if a partial volume effect is probable in our study, as in previous vascular PET studies in mice [10, 11, 14]. We did not characterize the composition of the atherosclerotic lesions, and we were unable to analyze the colocalization of immunostaining. Also, the ketogenic diet could not induce complete suppression of myocardial uptake and potential spillover into the ascending thoracic aorta cannot be excluded, although the myocardial uptake was similar between groups. In addition, the gamma counting of aortic ^{18}F-FDG uptake was similar between groups. We used the intraperitoneal route instead of the more commonly used intravenous route. However, the pharmacokinetics of the intraperitoneal route is similar to the intravenous route, provided that the PET acquisition is performed more than 60 min after ^{18}F-FDG administration [22]. In addition, the intraperitoneal route allows injecting conscious mice, a condition that further decrease ^{18}F-FDG myocardial uptake [20]. We were also unable to obtain enough blood from each mouse to carry out all the necessary analyses, affecting statistical power. However, biological results in these mice have previously been well studied [8–13, 15, 17–19, 30, 44, 45, 47, 53–56].

Conclusions

This first comparative study, with a dual staining and metabolic imaging assessment, of two frequently used methods of accelerated atherosclerosis in predisposed *ApoE*$^{-/-}$ mice provided two major results with their own consequences. First, ^{18}F-FDG PET-MR imaging at the 8-week follow-up failed to reveal an early atherogenic remodeling of the aorta that was nevertheless demonstrated using immunostaining. Second, only WD, and not uremia, significantly led to accelerated atherosclerosis, at least in its inflammatory component. Therefore, future studies with new anti-inflammatory and targeted therapies in *ApoE*$^{-/-}$ mice should use a WD to accelerate (inflammatory) atherosclerosis and should not rely solely on ^{18}F-FDG PET to assess the efficacy. Other possible discriminating imaging approaches could be proposed, such as other radiotracers than ^{18}F-FDG or micron-sized particles of iron oxide conjugated with antibodies targeting early endothelial activation and/or mineralization processes involved in atherosclerosis.

Supplementary Information The online version contains supplementary material available at https://doi.org/10.1007/s10554-024-03238-0.

Acknowledgements We thank Maelle GUYOT and Nicolas ELIE from the VIRTUAL'HIS platform (US PLATON, Caen University) for their technical support.

Author contributions All authors made substantial contributions to the data acquisition, revised the article critically and gave final approval of the manuscript to be submitted. Study conception and design: SD, PR, HdB, AAo, AM. Acquisition of data: SD, PR, CS, PAD, CB, AAb, AM. Analysis and interpretation of data: SD, CB, AM, AAo.

Funding This work was supported by the French Government, managed by the National Research Agency (ANR) under the program "Investissements d'avenir" with the reference ANR-16-RHUS-0003. Alain Manrique is supported by a grant from the GCS G4 as part of the FHU-CARNAVAL project labeled by AVIESAN. The funding sources were not involved in the collection, analysis, and interpretation of data; in the writing of the report; and in the decision to submit the article for publication.

Data availability All raw data are available from the Open Science Framework database (https://doi.org/10.17605/OSF.IO/TDMY2).

Declarations

Ethical approval All animal procedures were approved by the regional animal ethics committee (Comité d'Éthique NOrmand en Matière d'EXpérimentation Animale, CENOMEXA 054, n°29982) and were performed in accordance with the European directive 2010/63/EU on the protection of animals used for scientific purposes and specific French laws (decree n°2013–118).

Competing interests The authors declare no competing interests.

References

1. Wolf D, Ley K (2019) Immunity and inflammation in atherosclerosis. Circ Res 124:315–327. https://doi.org/10.1161/CIRCRESAHA.118.313591

2. Nidorf SM, Fiolet ATL, Mosterd A et al (2020) Colchicine in patients with chronic coronary disease. N Engl J Med 383:1838–1847. https://doi.org/10.1056/NEJMoa2021372
3. Tardif J-C, Kouz S, Waters DD et al (2019) Efficacy and safety of low-dose colchicine after myocardial infarction. N Engl J Med 381:2497–2505. https://doi.org/10.1056/NEJMoa1912388
4. Ridker PM, Everett BM, Pradhan A et al (2019) Low-dose methotrexate for the Prevention of atherosclerotic events. N Engl J Med 380:752–762. https://doi.org/10.1056/NEJMoa1809798
5. Ridker PM, Everett BM, Thuren T et al (2017) Antiinflammatory therapy with Canakinumab for atherosclerotic disease. N Engl J Med 377:1119–1131. https://doi.org/10.1056/NEJMoa1707914
6. Rossi-Semerano L, Fautrel B, Wendling D et al (2015) Tolerance and efficacy of off-label anti-interleukin-1 treatments in France: a nationwide survey. Orphanet J Rare Dis 10:19. https://doi.org/10.1186/s13023-015-0228-7
7. Khan N, Abbas AM, Whang N et al (2012) Incidence of Liver Toxicity in Inflammatory Bowel Disease patients treated with methotrexate: a Meta-analysis of clinical trials. Inflamm Bowel Dis 18:359–367. https://doi.org/10.1002/ibd.21820
8. Zhang SH, Reddick RL, Piedrahita JA, Maeda N (1992) Spontaneous hypercholesterolemia and arterial lesions in mice lacking apolipoprotein E. Science 258:468–471. https://doi.org/10.1126/science.1411543
9. Nakashima Y, Plump AS, Raines EW et al (1994) ApoE-deficient mice develop lesions of all phases of atherosclerosis throughout the arterial tree. Arterioscler Thromb 14:133–140. https://doi.org/10.1161/01.atv.14.1.133
10. Hag AMF, Pedersen SF, Christoffersen C et al (2012) 18F-FDG PET imaging of Murine Atherosclerosis: Association with Gene expression of key molecular markers. PLoS ONE 7:e50908. https://doi.org/10.1371/journal.pone.0050908
11. Ahmed M, Tegnebratt T, Tran TA et al (2020) Molecular Imaging of Inflammation in a mouse model of atherosclerosis using a zirconium-89-Labeled probe. Int J Nanomed Volume 15:6137–6152. https://doi.org/10.2147/IJN.S256395
12. Zhao Y, Kuge Y, Zhao S et al (2008) Prolonged High-Fat Feeding enhances aortic ^{18} F-FDG and ^{99m} Tc-Annexin A5 uptake in apolipoprotein E-Deficient and wild-type C57BL/6J mice. J Nucl Med 49:1707–1714. https://doi.org/10.2967/jnumed.108.051847
13. Rucher G, Cameliere L, Fendri J et al (2019) Molecular imaging of endothelial activation and mineralization in a mouse model of accelerated atherosclerosis. EJNMMI Res 9:80. https://doi.org/10.1186/s13550-019-0550-5
14. Laurberg JM, Olsen AK, Hansen SB et al (2007) Imaging of vulnerable atherosclerotic plaques with FDG-microPET: no FDG accumulation. Atherosclerosis 192:275–282. https://doi.org/10.1016/j.atherosclerosis.2006.07.019
15. Plump AS, Smith JD, Hayek T et al (1992) Severe hypercholesterolemia and atherosclerosis in apolipoprotein E-deficient mice created by homologous recombination in ES cells. Cell 71:343–353. https://doi.org/10.1016/0092-8674(92)90362-g
16. Winkels H, Ehinger E, Vassallo M et al (2018) Atlas of the Immune Cell Repertoire in Mouse Atherosclerosis defined by single-cell RNA-Sequencing and Mass Cytometry. Circ Res 122:1675–1688. https://doi.org/10.1161/CIRCRESAHA.117.312513
17. Bro S, Bentzon JF, Falk E et al (2003) Chronic renal failure accelerates atherogenesis in apolipoprotein E–Deficient mice. J Am Soc Nephrol 14:2466–2474. https://doi.org/10.1097/01.ASN.0000088024.72216.2E
18. Ivanovski O, Nikolov IG, Davceva O et al (2015) Compared with radical nephrectomy, Nephron-sparing partial nephrectomy protects apolipoprotein E–deficient mice from atherosclerosis progression. Urology 85. https://doi.org/10.1016/j.urology.2015.02.004.:1215.e9-1215.e15
19. Bro S, Moeller F, Andersen CB et al (2004) Increased expression of adhesion molecules in uremic atherosclerosis in apolipoprotein-E-deficient mice. J Am Soc Nephrol 15:1495–1503. https://doi.org/10.1097/01.asn.0000128371.33195.7b
20. Thackeray JT, Bankstahl JP, Wang Y et al (2015) Clinically relevant strategies for lowering cardiomyocyte glucose uptake for 18F-FDG imaging of myocardial inflammation in mice. Eur J Nucl Med Mol Imaging 42:771–780. https://doi.org/10.1007/s00259-014-2956-7
21. Cussó L, Musteanu M, Mulero F et al (2019) Effects of a ketogenic Diet on [18F]FDG-PET imaging in a mouse model of Lung Cancer. Mol Imaging Biol 21:279–285. https://doi.org/10.1007/s11307-018-1233-8
22. Kim C, Kim IH, Kim S et al (2011) Comparison of the intraperitoneal, Retroorbital and per oral routes for F-18 FDG Administration as Effective Alternatives to Intravenous Administration in Mouse Tumor models using small animal PET/CT studies. Nucl Med Mol Imaging 45:169–176. https://doi.org/10.1007/s13139-011-0087-7
23. Kikinis R, Pieper SD, Vosburgh KG (2014) 3D slicer: a platform for subject-specific image analysis, visualization, and clinical support. In: Jolesz FA (ed) Intraoperative Imaging and image-guided therapy. Springer New York, New York, NY, pp 277–289
24. Kapur T, Pieper S, Fedorov A et al (2016) Increasing the impact of medical image computing using community-based open-access hackathons: the NA-MIC and 3D slicer experience. Med Image Anal 33:176–180. https://doi.org/10.1016/j.media.2016.06.035
25. Fedorov A, Beichel R, Kalpathy-Cramer J et al (2012) 3D slicer as an image computing platform for the quantitative Imaging Network. Magn Reson Imaging 30:1323–1341. https://doi.org/10.1016/j.mri.2012.05.001
26. Fedorov A, Clunie D, Ulrich E et al (2016) DICOM for quantitative imaging biomarker development: a standards based approach to sharing clinical data and structured PET/CT analysis results in head and neck cancer research. PeerJ 4:e2057. https://doi.org/10.7717/peerj.2057
27. Cilla M, Pérez MM, Peña E, Martínez MA (2016) Effect of Diet and Age on arterial stiffening due to atherosclerosis in ApoE–/– mice. Ann Biomed Eng 44:2202–2217. https://doi.org/10.1007/s10439-015-1486-1
28. Bankhead P, Loughrey MB, Fernández JA et al (2017) QuPath: open source software for digital pathology image analysis. Sci Rep 7:16878. https://doi.org/10.1038/s41598-017-17204-5
29. Liu J, Kerwin WS, Caldwell JH et al (2016) High resolution FDG-microPET of carotid atherosclerosis: plaque components underlying enhanced FDG uptake. Int J Cardiovasc Imaging 32:145–152. https://doi.org/10.1007/s10554-015-0739-2
30. Massy ZA, Ivanovski O, Nguyen-Khoa T et al (2005) Uremia accelerates both atherosclerosis and arterial calcification in apolipoprotein E knockout mice. J Am Soc Nephrol 16:109–116. https://doi.org/10.1681/ASN.2004060495
31. Blomberg BA, Thomassen A, Takx RAP et al (2014) Delayed 18F-fluorodeoxyglucose PET/CT imaging improves quantitation of atherosclerotic plaque inflammation: results from the CAMONA study. J Nucl Cardiol 21:588–597. https://doi.org/10.1007/s12350-014-9884-6
32. Wenning C, Kloth C, Kuhlmann MT et al (2014) Serial F-18-FDG PET/CT distinguishes inflamed from stable plaque phenotypes in shear-stress induced murine atherosclerosis. Atherosclerosis 234:276–282. https://doi.org/10.1016/j.atherosclerosis.2014.03.008
33. Fazio S, Babaev VR, Murray AB et al (1997) Increased atherosclerosis in mice reconstituted with apolipoprotein E null macrophages. Proc Natl Acad Sci USA 94:4647–4652. https://doi.org/10.1073/pnas.94.9.4647

34. Wu H, Gower RM, Wang H et al (2009) Functional role of CD11c $^{+}$ monocytes in Atherogenesis Associated with Hypercholesterolemia. Circulation 119:2708–2717. https://doi.org/10.1161/CIRCULATIONAHA.108.823740
35. Gutiérrez-Muñoz C, Méndez-Barbero N, Svendsen P et al (2020) CD163 deficiency increases foam cell formation and plaque progression in atherosclerotic mice. FASEB J 34:14960–14976. https://doi.org/10.1096/fj.202000177R
36. McLaren JE, Ramji DP (2009) Interferon gamma: a master regulator of atherosclerosis. Cytokine Growth Factor Rev 20:125–135. https://doi.org/10.1016/j.cytogfr.2008.11.003
37. Tyrrell DJ, Goldstein DR (2021) Ageing and atherosclerosis: vascular intrinsic and extrinsic factors and potential role of IL-6. Nat Rev Cardiol 18:58–68. https://doi.org/10.1038/s41569-020-0431-7
38. Kamari Y, Shaish A, Shemesh S et al (2011) Reduced atherosclerosis and inflammatory cytokines in apolipoprotein-E-deficient mice lacking bone marrow-derived interleukin-1α. Biochem Biophys Res Commun 405:197–203. https://doi.org/10.1016/j.bbrc.2011.01.008
39. Harry BL, Sanders JM, Feaver RE et al (2008) Endothelial cell PECAM-1 promotes atherosclerotic lesions in Areas of Disturbed Flow in ApoE-Deficient mice. Arterioscler Thromb Vasc Biol 28:2003–2008. https://doi.org/10.1161/ATVBAHA.108.164707
40. Zibara K, Chignier E, Covacho C et al (2000) Modulation of expression of endothelial intercellular adhesion Molecule-1, platelet–endothelial cell adhesion Molecule-1, and vascular cell adhesion Molecule-1 in aortic Arch lesions of apolipoprotein E–Deficient compared with wild-type mice. Arterioscler Thromb Vasc Biol 20:2288–2296. https://doi.org/10.1161/01.ATV.20.10.2288
41. Rival Y, Del Maschio A, Rabiet MJ et al (1996) Inhibition of platelet endothelial cell adhesion molecule-1 synthesis and leukocyte transmigration in endothelial cells by the combined action of TNF-alpha and IFN-gamma. J Immunol 157:1233–1241
42. Stewart RJ, Kashour TS, Marsden PA (1996) Vascular endothelial platelet endothelial adhesion molecule-1 (PECAM-1) expression is decreased by TNF-alpha and IFN-gamma. Evidence for cytokine-induced destabilization of messenger ribonucleic acid transcripts in bovine endothelial cells. J Immunol 156:1221–1228
43. Gisterå A, Hansson GK (2017) The immunology of atherosclerosis. Nat Rev Nephrol 13:368–380. https://doi.org/10.1038/nrneph.2017.51
44. Buzello M, Törnig J, Faulhaber J et al (2003) The apolipoprotein E knockout mouse: a model documenting accelerated atherogenesis in Uremia. J Am Soc Nephrol 14:311–316. https://doi.org/10.1097/01.ASN.0000045048.71975.FC
45. Ge S, Hertel B, Koltsova EK et al (2013) Increased atherosclerotic lesion formation and vascular leukocyte Accumulation in Renal Impairment are mediated by Interleukin-17A. Circ Res 113:965–974. https://doi.org/10.1161/CIRCRESAHA.113.301934
46. Jing YJ, Ni JW, Ding FH et al (2016) p-Cresyl sulfate is associated with carotid arteriosclerosis in hemodialysis patients and promotes atherogenesis in apoE–/– mice. Kidney Int 89:439–449. https://doi.org/10.1038/ki.2015.287
47. Phan O, Ivanovski O, Nguyen-Khoa T et al (2005) Sevelamer prevents Uremia-enhanced atherosclerosis progression in apolipoprotein E–Deficient mice. Circulation 112:2875–2882. https://doi.org/10.1161/CIRCULATIONAHA105.541854
48. Jonsson AL, Bäckhed F (2017) Role of gut microbiota in atherosclerosis. Nat Rev Cardiol 14:79–87. https://doi.org/10.1038/nrcardio.2016.183
49. Robertson SJ, Lemire P, Maughan H et al (2019) Comparison of co-housing and littermate methods for Microbiota standardization in mouse models. Cell Rep 27:1910–1919e2. https://doi.org/10.1016/j.celrep.2019.04.023
50. Caligiuri G, Nicoletti A, Zhou X et al (1999) Effects of sex and age on atherosclerosis and autoimmunity in apoe-deficient mice. Atherosclerosis 145:301–308. https://doi.org/10.1016/s0021-9150(99)00081-7
51. Meester EJ, Krenning BJ, de Swart J et al (2019) Perspectives on small animal Radionuclide Imaging; considerations and advances in atherosclerosis. Front Med (Lausanne) 6:39. https://doi.org/10.3389/fmed.2019.00039
52. McKenney-Drake ML, Moghbel MC, Paydary K et al (2018) 18F-NaF and 18F-FDG as molecular probes in the evaluation of atherosclerosis. Eur J Nucl Med Mol Imaging 45:2190–2200. https://doi.org/10.1007/s00259-018-4078-0
53. Phan O, Ivanovski O, Nikolov IG et al (2008) Effect of oral calcium carbonate on aortic calcification in apolipoprotein E-deficient (apoE-/-) mice with chronic renal failure. Nephrol Dial Transpl 23:82–90. https://doi.org/10.1093/ndt/gfm699
54. Ivanovski O, Szumilak D, Nguyen-Khoa T et al (2005) The antioxidant N-acetylcysteine prevents accelerated atherosclerosis in uremic apolipoprotein E knockout mice. Kidney Int 67:2288–2294. https://doi.org/10.1111/j.1523-1755.2005.00332.x
55. Bro S, Borup R, Andersen CB et al (2006) Uremia-Specific effects in the arterial media during development of uremic atherosclerosis in apolipoprotein E–Deficient mice. Arterioscler Thromb Vasc Biol 26:570–575. https://doi.org/10.1161/01.ATV.0000201060.47945.cb
56. Belmokhtar K, Ortillon J, Jaisson S et al (2019) Receptor for advanced glycation end products: a key molecule in the genesis of chronic kidney disease vascular calcification and a potential modulator of sodium phosphate co-transporter PIT-1 expression. Nephrol Dial Transpl 34:2018–2030. https://doi.org/10.1093/ndt/gfz012